UNIVERSIDADE DE SÃO PAULO

INSTITUTO DE FÍSICA
CAIXA POSTAL 20516
01498 - SÃO PAULO - SP
BRASIL

PUBLICAÇÕES

IFUSP/P-700

LINE SHAPE AND THERMAL KINETICS ANALYSIS OF THE Fe^{2+}-BAND IN BRAZILIAN GREEN BERYL

Sadao Isotani, Wagner W. Furtado, Rodolfo Antonini and Osvaldo Luis Dias

Instituto De Física, Universidade de São Paulo

Março/1988

LINE SHAPE AND THERMAL KINETICS ANALYSIS OF THE Fe^{2+}-BAND IN BRAZILIAN GREEN BERYL

Sadao Isotani, Wagner W. Furtado, Rodolfo Antonini and Osvaldo Luis Dias

Instituto de Física, Universidade de São Paulo
C.P. 20516, 01498 São Paulo, SP, Brazil

Key words: Beryl, Optical Absorption, Line Shape, Thermal Kinetics.

ABSTRACT

The optical absorption spectra study through isothermal treatments of the σ- and π-polarized bands of Fe^{2+}-band is reported. It was shown a linear correlation between these bands through thermal treatments. Irradiation with γ-rays from ^{60}Co, showed the decrease of this band. The line shape analysis and the discussions lend us to assign the π- and σ-polarized bands to Fe^{2+} ions in the structural channels with and without neighbour water molecules, respectively. The kinetics analysis through a "bimolecular-like" model gives untrapping parameter with Arrhenius behavior. The retrapping and recombination parameters showed a behavior proportional to $T^{\frac{1}{2}} - T_o^{\frac{1}{2}}$, which were explained from free electron distribution of velocities and minimum untrapped electron energy due to a potential barrier of the trap. The kinetics cut-off temperacure, T_o, agrees with the previous experimental observation.

I. INTRODUCTION

Beryl is a cyclo-silicate crystal with the chemical formula $Be_3Al_2Si_6O_{18}$ (Dana and Hurlbut, 1978). The coordination structure was determined by Bragg and West (1926). It belongs to the hexagonal system and the unit cell is composed by two $Be_3Al_2Si_6O_{18}$ molecules. The axial parameters of high purity beryl crystal are: $\underline{c}$ = 9.17 ± 0,01 Å and $\underline{a}$ = 9.20 ± 0.01 Å. These parameters are changed by the presence of alkali ions in the crystal lattice (Bakakin et al., 1967). Beryl belongs to P6/mcc space group. The Si_6O_{18} rings form structural channels parallel to the crystallographic axis. The effective diameter of these structural channels varies from 2.8 Å in the Si_6O_{18} ring plane to 5.1 Å in the middle of two neighbouring rings, respectively.

The blue color of natural beryl (aquamarine) is due to absorption bands in the near infrared. These bands were unanimously assigned to Fe^{2+} impurity (Wood and Nassau, 1968; Samoilovich et al., 1971; Price et al., 1976; Parkin et al., 1977; Goldman et al., 1978; Bak et al., 1982). Several bands in the near infrared were reported: A-band around ~12,000 cm^{-1} observed for the

incident light bean perpendicular to the $\underline{c}$-axis ($\underline{k} \perp \underline{c}$); B-bands composed by two bands around ~12,000 and ~10,000 cm^{-1} ($\underline{k} // \underline{c}$); C-band around ~16,000 cm^{-1} ($\underline{k} // \underline{c}$). The Mossbauer spectra of several samples showed the presence of the two Fe^{2+} sites.

The A-band was firstly assigned to Fe^{2+} in the six-coordinated Al^{3+} site (Wood and Nassau, 1968; Samoilovich et al., 1971; Parkin et al., 1977). Price et al. (1978) on examining the OA, Mossbauer and ESR spectra assigned the A-band to Fe^{2+} in tetrahedral site and the B-bands to Fe^{2+} in the Al^{3+} site. The deficciences of these assignments were pointed out by Goldman et al. (1978), which on examining the OA and Mossbauer spectra of several samples of beryl reached to the conclusion that: A-band is due to Fe^{2+} in the structural channels; B-bands are due to Fe^{2+} in six-fold symmetry site; C-band is due to the intervalence charge transfer between Fe^{2+} and Fe^{3+} ions.

The IR, OA and EPR studies of green and blue beryl from Minas Gerais, Brazil (Blak et al., 1982) showed that Fe^{2+}, Fe^{3+}, alkali and water impurities occupies different sites in the two samples. As only the A-band was present in the OA spectra of these samples, it shows

that Fe^{2+} ions are in the structural channels. The EPR spectra showed the presence of Fe^{3+} ions in the channels of green beryl and Fe^{3+} ions at the $A\ell^{3+}$ site in green and blue beryl. Thermal treatments above 200°C in green beryl showed the growth of the A-band and the bleaching of the EPR signal of Fe^{3+} ion, is followed by the change of color to blue. The correlation between the A-band growth and EPR signal bleaching was shown to be linear. On the other hand, the thermal treatment above 200°C of blue beryl does not change the A-band nor the EPR lines of the Fe^{3+} ions at the $A\ell^{3+}$ sites, and the color remains unchanged. This shows that the Fe^{3+} ions at the $A\ell^{3+}$ sites are not oxidized into Fe^{4+}.

The purpose of the present work is the analysis of the A-band in the beryl samples studied previously by Blak et al. (1982) and Dias (1981), through the line shape analysis of the σ- and π-polarized spectra and the analysis of the kinetic mechanism of the A-band.

II. EXPERIMENTAL

The samples of green and colorless beryl were

obtained in Minas Gerais, Brazil and were studied previously by Blak et al. (1982) and Dias (1981). The samples were cut in the form of parallelopipeds with two faces perpendicular and parallel to the c-axis, with about 5 mm of thickness.

A Carl-Zeiss DMR 21 spectrophotometer was used for the optical absorption measurements. Polarized light measurements were done with Type II polaroid.

The thermal treatments were done in air. The stability of the furnace with useful volume 10 × 12 × 15 cm was improved to 1°C by filling with brick materials and two metallic plates. The temperature was measured using a chromel-alumel termocouple, with one junction at 0°C with ECB X-T recorder and a Keithley 160B digital multimeter. All the samples to be treated were put between previously heated metallic plates. With this set thermal equilibrium was achieved in the samples in about 40 seconds (Dias, 1981).

The samples were γ-irradiated using a ^{60}Co-source (~ 400,000 Ci) from EMBRARAD S.A.. The dose was controlled by means of three processes: Ceric-Cerous dosimetric system, AECL Red Acryllic dosimetric system and UKAEA Red Perspex dosimeter.

III. RESULTS

In figure 1 we show the polarized spectra

Insert Figure 1

of green beryl for $\vec{k} \perp$ c-axis at around 12,000 cm^{-1}. The σ-band ($\vec{E} \perp$ c-axis) is at about 11,750 cm^{-1} and the π-band ($\vec{E} //$ c-axis) is at about 12,750 cm^{-1}.

The band position at around 12,000 cm^{-1} change from 11,750 cm^{-1} (σ-band, $\vartheta = 90^{o}$) to 12,750 cm^{-1} (π-band, $\vartheta = 0^{o}$) with the electrical field direction measured as the angle ϑ between the electrical field and the c-axis. The band-position variation with ϑ is shown in figure 2.

Insert Figure 2

The deformation in the 180^{o} symmetry, probably, is because the sample was not cut with enough accuracy. The σ- and π-polarized band positions were not changed on heating 600^{o}C.

In figure 3 we show the growth-curves of the σ-polarized bands for the isothermal treatments at 411^{o}, 492^{o}, 525^{o} and 600^{o}C. The growth curves were shown as

$I/I_{o} - 1$ versus irradiation dose, where I is the optical absorption intensity and I_{o} is the optical absorption intensity of unheated green beryl.

Insert Figure 3

In figure 4, we show the correlation between the areas of the σ- and π-polarized bands of green beryl

Insert Figure 4

submitted to the isothermal treatments at 411^{o}, 492^{o} and 600^{o}C. We see that the correlation is linear.

The irradiation of 600^{o}C heated green beryl of blue-color, turns it green again. The UV band-edge shifts to the blue region of the spectrum and the σ- and π-bands decreases. In figure 5, we show the decrease of

Insert Figure 5

the unpolarized $\vec{k} //$ c-axis band at around 12,000 cm^{-1} of a colorless beryl irradiated with γ-rays. The decay curve is normalized to the band intensity of the non-irradiated sample.

IV. THE LINE SHAPE ANALYSIS

The line shape analysis of the σ- and π-polarized bands were done using normalized bands for natural and 600°C heated green beryl samples. The plot is with the relative wavenumber $\nu = \nu - \nu_o$, where ν is the wavenumber and ν_o is the wavenumber at the maximum absorbance. In figure 6 we show these bands. The line shape of the

Insert Figure 6

σ-polarized band does not change on heating at 600°C and show a line width of 960 cm^{-1}. Also, the line shape of the π-polarized band is not changed on heating at 600°C and show a line width of 1200 cm^{-1}.

We assume the Gaussian line shape model for the present line shape analysis. For this purpose we define tne gaussian-functions:

$$f_\sigma = \exp\left\{ - \ell n^2 \frac{(\nu - 11,750)^2}{960} \right\} , \qquad (1)$$

$$f_\pi = \exp\left\{ - \ell n^2 \frac{(\nu - 12,750)^2}{1,200} \right\} . \qquad (2)$$

The fit with these functions is shown in figure 6 for f_σ and for f_π. We see that this model gives a good result.

The above determined line shapes for the σ- and π-polarized bands makes possible the evaluation of the dependence of the band positions with the electrical field direction of the light beam measured in angles between $\vartheta = 0$ for π-polarization and $\vartheta = 90^o$ for σ-polarization. By assuming the Malu's law for the polarization dependence on angle, we have for the A-band line-shape:

$$F(\nu) = A \, sen^2\vartheta \, f_\sigma(\nu) + B \cos^2\vartheta \, f_\pi(\nu) , \qquad (3)$$

For $\vartheta = 0$ $F(\nu) = B \, f_\sigma(\nu)$ and for $\vartheta = 90^o$ $F(\nu) = A \, f_\sigma(\nu)$. From the spectra reported by Dias (1981) we obtained B = 2A. The band position, ν_m, is obtained at the maximum of the $F(\nu)$ line shape. This maximum is determined by equating to zero the first derivative of $F(\nu)$. The resultant equation:

$$sen^2\vartheta \frac{(\nu_m - 11,750)}{960^2} f_\sigma + 2 \cos^2\vartheta \frac{(\nu_m - 12,750)}{1200^2} f_\pi = 0 \qquad (4)$$

is a transcedental equation relating ν_m with ϑ. The result of the calculation of ν_m with ϑ using the above equation is shown in figure 6 solid line. This shows a good agreement with the experimental data.

In figure 7, we show the non-polarized OA band around 12,000 cm^{-1} for $\underset{\sim}{k}//\underset{\sim}{c}$-axis of green and blue

Insert Figure 7

beryl reported by Blak et al. (1982). The asymmetry of this band was assigned to be resultant from two Gaussian lines at ~12,000 cm^{-1} (line I) and ~13,000 cm^{-1} (line II). The σ- and π-polarized bands analysed here are consistent with the lines I and II proposed previously. We analysed this assignment by fitting the band at figure 3 as sum of the lines σ and π. A good fit was obtained using the equations:

$$F\ (\text{green}) = 0.526 + 12{,}3\ 10^{-6}\ \nu + 0.176\ f_\sigma + 0.144\ f_\pi \quad , \tag{5}$$

$$F\ (\text{blue}) = 0.238 + 46.9\ 10^{-6}\ \nu + 0.148\ f_\sigma + 0.432\ f_\pi \quad , \tag{6}$$

as shown in figure 7.

The intensities of the σ- and π-lines are given by the coefficients of the equations 5 and 6. The ratio between the intensities of the π- and σ-lines are: 0.8 for green beryl and 2.9 for blue beryl. We see that the ratio is larger for blue beryl. This suggests that the π- and σ-polarized lines are due to two different centers.

V. KINETICS

The kinetics of the reduction of Fe^{3+} into Fe^{2+} was firstly determined by Blak et al. (1982) for green beryl. An empirical analysis of the kinetics using a sum of two first-order processes (Levy et al., 1974) showed activation energies 0.30 and 0.46 ev. Also, it was shown that at room temperature the half-life of Fe^{3+} was 7.5 and 1.5 years, respectively. These results indicate that no green beryl should be found in nature. Since this is not true it was concluded that there is a minimum temperature necessary for the reduction of Fe^{3+} into Fe^{2+}. Thus, by measuring $I(t_{\frac{1}{2}})/I(t=0)$ at several

temperatures below 400°C, it was shown that the Fe^{3+} reduction into Fe^{2+} stop at about 200°C.

As the empirical model does not explain the stop of the kinetics, we develop at the present an study of the Blak et al. (1982) data using the method reported by Furtado (1986). Also, Blak's previous analysis using the sum of two first-order kinetics makes easy the comparison between the two methods.

Here we assume a model where Fe^{3+} is reduced into Fe^{2+}, thorugh the thermal induced release of holes from Fe^{3+} ions into the valence band. Also, it was assumed that these valence holes recombine with electron trapped at a single deep trapping center. In figure 8, we show a sketch of the process proposed here.

Insert Figure 8

The process a is the result of the thermal reduction of Fe^{3+} ion into Fe^{2+} ion through the release of a hole into the valence band. The process b is the capture process (oxidation) of a valence hole by Fe^{2+} ion giving Fe^{3+} ion, a process, which we call retrapping of a hole. The process c is the electron-hole annihilation

in the R center, which we call recombination of a hole. The R center, is a center produced by the capture of electron in a crystal defect giving a deep level. The kinetic equations, using the "bimolecular-like" model (Furtado, 1986) are:

process a:

$$\frac{d}{dt}[Fe^{3+}] = -\frac{d}{dt}[Fe^{2+}] = -\frac{d}{dt}[h^{+}] = -\alpha[Fe^{3+}] \qquad (7a)$$

process b:

$$\frac{d}{dt}[Fe^{2+}] = \frac{d}{dt}[h^{+}] = -\frac{d}{dt}[Fe^{3+}] = -\gamma[Fe^{2+}][h^{+}] \qquad (7b)$$

process c:

$$\frac{d}{dt}[h^{+}] = \frac{d}{dt}[R^{-}] = -\frac{d}{dt}[R] = -\beta[R^{-}][h^{+}] \quad , \qquad (7c)$$

where the brakets means the concentrations, h^{+}, holes in the valence band. The parameter α is related to the probability of hole untrapping, thus obeying the Arrhenius' law. The parameters γ describes retrapping and β describes the electron-hole recombination.

From equations (7) we obtain the equations for the kinetic process proposed for the production of Fe^{3+} into Fe^{2+}. They are:

$$\frac{d}{dt}[Fe^{3+}] = -\alpha[Fe^{3+}] + \gamma[Fe^{2+}][h^+] \quad , \tag{8a}$$

$$\frac{d}{dt}[Fe^{2+}] = \alpha[Fe^{3+}] - \gamma[Fe^{2+}][h^+] \quad , \tag{8b}$$

$$\frac{d}{dt}[R^-] = -\beta[R^-][h^+] \quad , \tag{8c}$$

$$\frac{d}{dt}[R] = \beta[R^-][h^+] \quad , \tag{8d}$$

$$\frac{d}{dt}[h^+] = \alpha[Fe^{3+}] - \gamma[Fe^{2+}][h^+] - \beta[R^-][h^+] \quad . \tag{8e}$$

Some of the above equations are coupled through the conditions:

(i) the total iron concentration available for the reactions is constant:

$$[Fe]_0 = [Fe^{3+}] + [Fe^{2+}] \quad , \tag{9a}$$

(ii) the charge distribution is:

$$[R^-] = [Fe^{3+}] + [h^+] \quad . \tag{9b}$$

Then, we obtain the following equations:

$$\frac{d}{dt}[Fe^{2+}] = \alpha\left\{[Fe]_0 - [Fe^{2+}]\right\} - \gamma[Fe^{2+}][h^+] \quad , \tag{10a}$$

$$\frac{d}{dt}[h^+] = \frac{d}{dt}[Fe^{2+}] - \beta\left\{[Fe]_0 - [Fe^{2+}] + [h^+]\right\}[h^+] . \tag{10b}$$

These equations were evaluated for Fe^{2+} using the method of Runge-Kutta, following the procedures described by Furtado (1986). The normalization of the above equations were done on the initial concentration of Fe^{2+}, giving the initial conditions, $[Fe^{2+}](0) = 1$ and $[h^+](0) = 0$.

The parameters for the best fit curves shown in figure 3, are shown in table 1.

Insert Table 1

The parameter α follows the Arrhenius law as shown in figure 9. The fit gives for the activation energy $\Delta E = 1.03$ ev and the frequency factor is $4.74 \times 10^7 s^{-1}$.

Insert Figure 9

The parameters $C = \gamma/[Fe^{2+}](0)$ and $B = \beta/[Fe^{2+}](0)$ showed a linear correlation with $T^{\frac{1}{2}}$, as shown in figure 10. The parameters correlation with $T^{\frac{1}{2}}$ also shows that there is a temperature $T_0 \simeq 473^{o}K$, where these parameters turns zero. This means that the kinetic process, which concerns to

Insert Figure 10

retrapping and R electron-hole recombination ceases. Thus we call T_0 as kinetics cut-off temperature.

The present analysis for B and C behavior with temperature agrees well with the Blak et al. (1982) observation that Fe^{3+} reduction into Fe^{2+} stop at about $200^{o}C$.

VI. DISCUSSION

Irradiation of colorless beryl from Minas Gerais, Brazil, showed the oxidation of Fe^{2+} into Fe^{3+}. On the other hand, Blak et al. (1982), through OA and EPR studies of blue beryl, showed that Fe^{3+} in Al^{3+} substitutional sites are not reduced on heating while

Fe^{3+} at the channels are reduced. These observations showed that oxi-reduction process occur only for Fe in the structural channels. Also, due to different relative contribution of the σ- and π-polarized lines in blue and green beryl we suggest that the A-band is composed by the absorbances of Fe^{2+} ions at two different sites in the structural channels.

Now if the Fe^{2+} are in the structural channels, we have to explain the apparently contradictory observations: similar kinetics for σ- and π-polarized OA bands as shown in figure 3; different relation between the σ- and π-polarized lines for $\underline{k}//\underline{c}$-axis measurements in blue and green beryl.

It was shown by Wood and Nassau (1968) that water molecules in beryl occupy two sites in structural channels. The water in site I (type I) have its C_2 symmetry axis perpendicular to the crystal $\underline{c}$-axis and the water in site II (type II) have its C_2 symmetry axis parallel to the crystal $\underline{c}$-axis. The type I water molecule is predominant in blue while type II water molecule is predominant in green beryl (Blak et al., 1982).

Ions of Fe can be found in the structural channels at least: (i) without neighbour water molecule;

(ii) with neighbour type II water molecule. The crystal field symmetry of Fe^{2+} water free ion will be different of that water associated Fe ion.

Type II water molecules, because the oxygen atom of the water molecule is near to the Fe^{2+} ion will increase the dipole moment along the c-axis giving absorbance maximum for $\underline{E}//c$-axis, i.e., the π-polarized line. The Fe^{2+} water free ion have the dipole moment due to the local cage of oxygen atoms. Due to the channel structure of the oxygen piling the crystal field have its maximum perpendicular to the c-axis, and so the dipole moment will be perpendicular to the c-axis, giving absorbance maxima for $\underline{E} \perp c$-axis, i.e., the σ-polarized line.

The irradiation induced Fe^{2+} oxidation, probably, is due to the capture of hole from the valence band, allowed to interact with Fe^{2+} through the O^{2-} ions of the structural channels. So, possibly, the presence of water near Fe^{2+} does not changes the hole capture cross section. Otherwise, the Fe^{3+} thermal reduction into Fe^{2+}, possibly, is due to the thermal release of a hole through the O^{2-} ions of the structural channels. So, the kinetics of reduction of Fe^{3+} into Fe^{2+} is expected to be similar

for both Fe^{2+} with and without neighbouring water molecules. In this way, the kinetics of Fe^{2+} in sites giving σ- and π-polarized absorption bands are expected to be similar.

In blue beryl alkali content is small as shown by the predominant type I water molecules. This situation is good for the association of Fe^{2+} ions with water molecules. So, in blue beryl the π-polarized line is expected to be the biggest.

In green beryl alkali content is high, as shown by the predominant type II water molecule. This makes smaller the possibility of association of Fe^{2+} with water molecules, thus giving bigger A_σ/A_π relation, as compared to blue beryl.

The presence of π-polarized band in the $\underline{k}//c$-axis spectra is allowed if we assume magnetic dipole transition. The π-polarized spectra appears for $\underline{E}//c$-axis. In this case the magnetic field radiation, $\underline{H}$, is perpendicular to the c-axis. For $\underline{k}//c$-axis, $\underline{H}$, is also perpendicular to the c-axis, while $\underline{E}$ being perpendicular to the c-axis does not allow π-polarized spectrum. Magnetic dipole process is a weaker process, since the maximum possible values of the matrix elements $\langle f|\underline{\mu}.\underline{B}|i\rangle$ (i,f =

initial and final states, $\underline{\mu}$ = magnetic dipole operator, $\underline{B}$ = the strength of the magnetic field radiation) are smaller than the possible values of the matrix elements of $\langle f|\underline{p}.\underline{E}|i\rangle$ ($\underline{p}$ = electric dipole moment operator). Thus, when a radiative transition is forbidden by an electric dipole process (Imbusch, 1978, p. 23) it may occur an magnetic dipole process. This is consistent with the assignment of the A-band to the d-d electrical dipole forbidden transition of Fe^{2+} (in octahedral symmetry d-orbitals are symmetric and so $\langle f|\underline{p}.\underline{E}|i\rangle = 0$). This band is allowed by distortion of the crystal field.

The activation energy determined by us is 1.03 ev, in contrast with those obtained by Blak et al. (1982) in the two single first-order approximation of Levy et al. (1974), where it was obtained two activation energies: 0.46 and 0.3 ev. This means that the present activation energy value is at least twice of the previous ones. We assign the difference to the inclusion of recombination process which delay the kinetics, increasing the activation energy in the fit. The Blak et al. method using the equation:

$$I(t) = a_1 \exp(-b_1 t) + a_2 \exp(-b_2 t) \quad , \qquad (11)$$

obtained parameters a_1 and a_2 depending of temperature. However, being each exponential, a first-order kinetics of a single center, the expected behavior for a_1 and a_2 are to be constant with temperature. Finally we would like to point out that the cut-off temperature, available for the parameters B and C, are not expected for a_1 and a_2.

The $T^{\frac{1}{2}}$ behavior is the result of free electron model. Let us consider N conduction electrons which through collisions with another N' hole centers, removes one electron per collision from the set N. Thus, the change in N, dN, when the electrons travel a distance dx is given by (Sears, 1963; p. 259):

$$dN = -PNdx \quad , \qquad (12)$$

where $\underline{P}$ is the collision probability and which is given by the product of the hole-center collision cross section, σ, with the number of centers, N'. Here, N is the number of holes at a certain instant, dN the number of holes which make collisions and be removed from the group after this group have traveled a distance dx. Assuming that the holes travel with speed v in a time interval

dt , we obtain the rate equation:

$$\frac{dN}{dt} = -\underline{P}\,Nv \quad . \tag{13}$$

The group of N holes have different speeds. The rate equation for N_i holes with speed v_i is:

$$\frac{d\Delta}{dt} N_i = -P\,\Delta N_i\, N_i \quad . \tag{14}$$

The sum over all possible groups of speed gives the rate equation for N :

$$\frac{d}{dt} N = -\sum_i \underline{P}\,\Delta N_i\, v_i \quad . \tag{15}$$

Then for $\Delta N_i \to 0$, we obtain:

$$\frac{d}{dt} N = -\int_{all} P\,v\,dN \quad . \tag{16}$$

The holes in the valence band behaves nearly like free particles. Thus we assume for dN the free particles distribution (Sears, 1963; p. 235):

$$dN = \frac{4N}{\sqrt{\pi}} \left(\frac{m}{2kT}\right)^{3/2} v^2 \exp\left(-\frac{mv^2}{2kT}\right) dv \quad . \tag{17}$$

Evaluating the rate equation for this distribution and using the definition of P , we obtain:

$$\frac{dN}{dt} = -\sigma\,\bar{v}\,N N' \quad , \tag{18}$$

where

$$\bar{v} = \sqrt{\frac{8kT}{\pi m}} \quad .$$

The existence of a cut-off temperature shows the lattice microscopic structure. We expect small local variations in the valence band potential, with differences of around decimal electron-volts, because of the negative character of the Fe^{2+} , which attract holes of the neighbours, giving rise to a potential barrier.

Holes which are released from the capture centers with an energy smaller than the potential barrier will find potential maxima which will delay the propagations of the holes. On the other hand, these electrons are released through tunneling, giving a small concentrations of these holes, as related to the thermally released holes. From this, the kinetics of these delayed holes have a few contribution to the kinetics.

The holes thermally released will have an energy K_0, above the maxima of the potential of the valence band. This energy gives rise to a minimum velocity $v_0 = \sqrt{2K_0/m}$ for the holes. This implies that there will not be holes with $v < v_0$, changing the distribution proposed above. We suggest that this phenomenon gives rise to a speed screening:

$$\frac{dN}{dt} = -\sigma(v-\bar{v}_0)\, N\bar{N}' \quad . \qquad (19)$$

Assuming for $v_0 = \sqrt{8kT_0/\pi m}$ we obtain

$$\frac{dN}{dt} = \text{ctte}\ (\sqrt{T} - \sqrt{T_0})\, NN' \qquad (20)$$

found for B and C. This relation agrees with the present analysis for the kinetics of the reduction of Fe^{3+} into Fe^{2+}.

ACKNOWLEDGMENTS

We would like to thanks Prof. Clemencio Teodoro Dotto for his collaboration in the computation part of this work. This work was partly supported by grants from CAPES-PICD, CNPq, FINEP and FAPESP.

REFERENCES

Bakakin, V.V. and Rylov, G.M. (1967) Correlation between the chemical composition and unit cell parameteres of beryl. Doklady Academie S.S.S.R., 173, 129-132.

Bragg, W.L. and West, J. (1926) The structure of beryl $Be_3Al_2Si_6O_{18}$. Proceedings of Royal Society of London Ser. A, 111, 691-714.

Blak, A.R., Isotani, S., Watanabe, S. (1982) Optical absorption and electron spin resonance in blue and natural beryl. Physical Chemistry of Minerals, 8, 161-166.

Dana, J.M. and Hurlbut Jr., C.S. (1978) Dana's manual of mineralogy. Livros Técnicos e Científicos, Rio de Janeiro.

Dias, O.L. (1981) Study of beryl with X-ray fluorescence and optical absorption spectroscopy. Ms.Sc. Thesis, University of São Paulo, SP, Brazil.

Furtado, W.W. (1986) Analysis of the Interstitial Atomic Hydrogen Kinetics in a-Si:H and beryl. Ms.Sc. Thesis, University of São Paulo.

Imbusch, G.F. (1978) Inorganic Luminescence - In Luminescence Spectroscopy, Lumb, M.D. (Ed.), Academic Press, London, New York, San Francisco.

Goldman, D.S., Rossman, G.R., and Parkins, K.M. (1978) Channel constituents in beryl. Physics and Chemistry of Minerals, 3, 225-235.

Levy, P.W., Mattern, P.L., Lengweiler, K., and Bishay, A.M. (1974) Studies on nonmetals during irradiation: V, growth and decay of color centers in barium alumino-borate glasses containing Cerium. Journal of American Ceramic Society, 57, 176-181.

Parkins, K.M., Loefler, B.M., and Burns, R.G. (1977) Mossbauer spectra of kianite, aquamarine and cordierite showing intervalence charge transfer. Physics and Chemistry of Minerals, 1, 301-311.

Price, D.C., Vance, E.R., Smith, G., Edgar, A. and Dickson, B.L. (1976) Mossbauer effect studies of beryl. Journal de Physique, 37, Colloque C, Supplement 12, 147-150.

Samoilovich, M.I., Tsinober, L.I., and Dunin-Barkoviskii, K.L. (1971) Nature of coloring in iron containing beryl. Sov. Phys. Cryst., 16, 147-150.

Sears, F.W. (1963) Thermodynamics, the kinetic theory of gases and statistical mechanics. Addison-Wesley Publ. Co, Inc., Reading, Massachussets, Palo Alto, London.

Wood, D.L. and Nassau, K. (1968) The characterization of beryl and emerald by visible and infrared absorption spectroscopy. American Mineralogist, 53, 777-800.

Table 1 - Parameters fif for the kinetic equations (16) for Fe^{2+} OA-band in brazilian green beryl.

T (K)	α	C	B	N
673	1.00 $^{+0.15}_{-0.10}$	29 $^{+1}_{-1}$	9.8 $^{+1.2}_{-0.8}$	1.90 $^{+0.01}_{-0.01}$
723	3.5 $^{+0.5}_{-0.1}$	35.6 $^{+0.4}_{-1.6}$	12 $^{+2}_{-1}$	2.00 $^{+0.01}_{-0.01}$
763	4.8 $^{+0.1}_{-0.3}$	42 $^{+1}_{-1}$	12 $^{+1}_{-1}$	2.90 $^{+0.01}_{-0.01}$
823	23 $^{+1}_{-1}$	48.5 $^{+0.5}_{-0.5}$	15.5 $^{+1.0}_{-1.0}$	3.50 $^{+0.01}_{-0.01}$
873	59 $^{+1}_{-1}$	54.0 $^{+0.5}_{-0.5}$	18 $^{+1}_{-1}$	4.23 $^{+0.01}_{-0.01}$

FIGURE CAPTIONS

Figure 1 - σ-($\vec{E} \perp$ c-axis) and π-($\vec{E}$//c-axis) polarized spectra of green beryl at around 12,000 cm^{-1} (A-band).

Figure 2 - A-band maxima versus $\vec{E}$ for $\vec{k} \perp$ c-axis (• experimental; —— calculated).

Figure 3 - Normalized ($I/I_o - 1$) intensities of the σ-polarized band for isothermal treatments at 411°, 492°, 525° and 600°C (• experimental; —— calculated).

Figure 4 - Correlation between the areas of the σ- and π-polarized bands for isothermal treatments at 411°, 492° and 600°C.

Figure 5 - Normalized (I/I_o) intensities of the A-band for $\vec{k}$//c-axis versus irradiation dose (γ-Rays from ^{60}Co).

Figure 6 - Fit of the line shapes of the σ- (—— unheated; —·—·— heated at 600°C; • calculated) and π- (···· unheated; ----- heated at 600°C; ▲ calculated).

Figure 7 - Fit of the line shape of the A-band for $\vec{k} \perp$ c-axis (—— experimental; • calculated).

Figure 8 - Sketch of the kinetic processes.

Figure 9 - Parameter α versus 1/T showing Arrhenius law.

Figure 10 - Parameters B and C showing $T^{\frac{1}{2}}$ dependence.

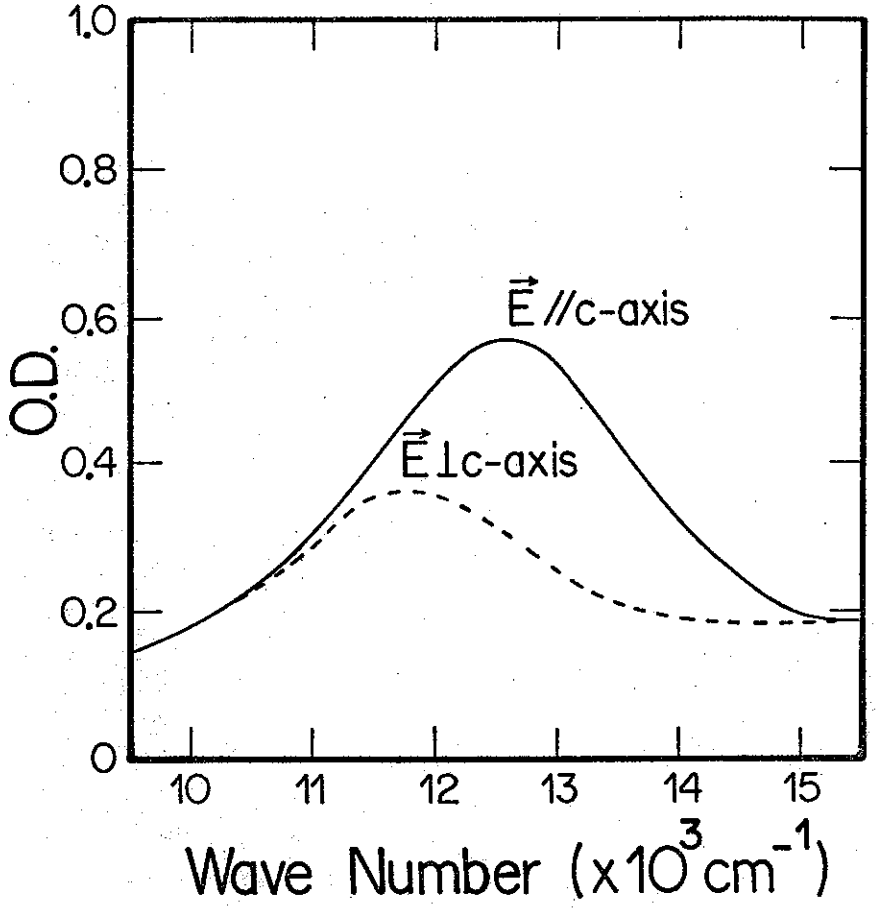

FIGURE 1

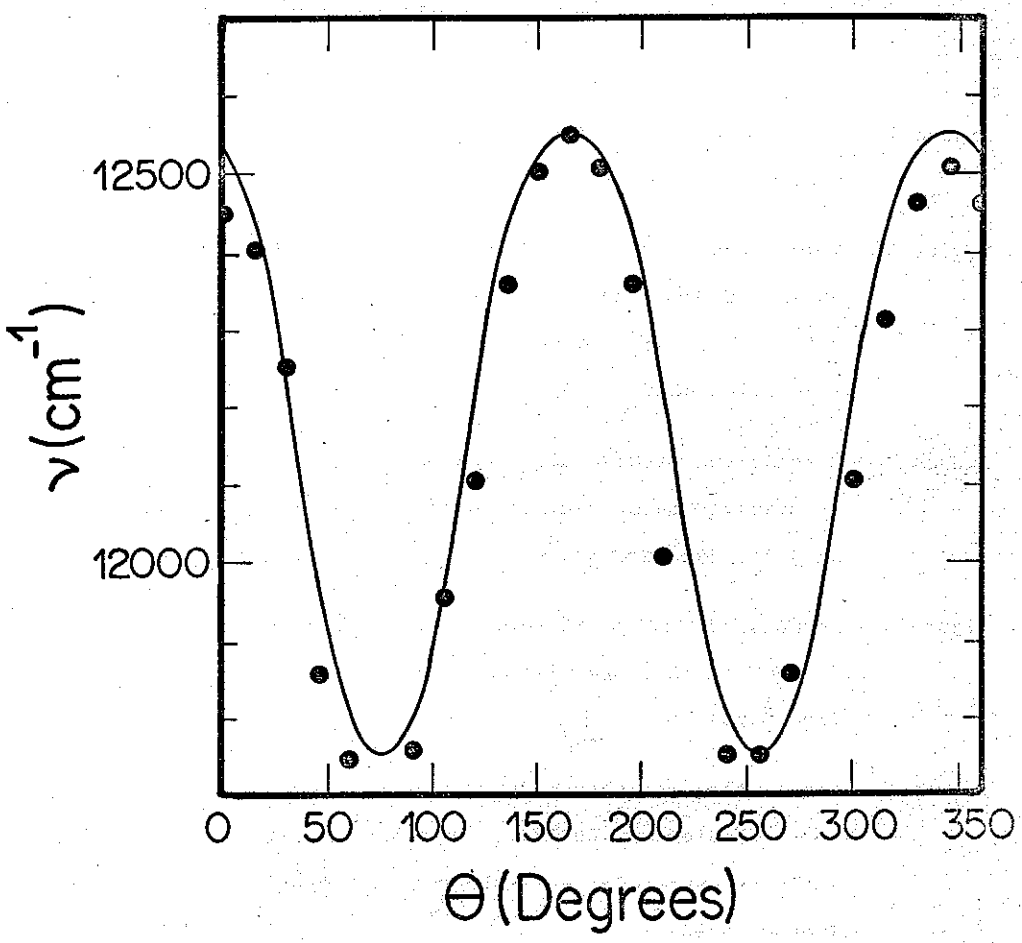

FIGURE 2

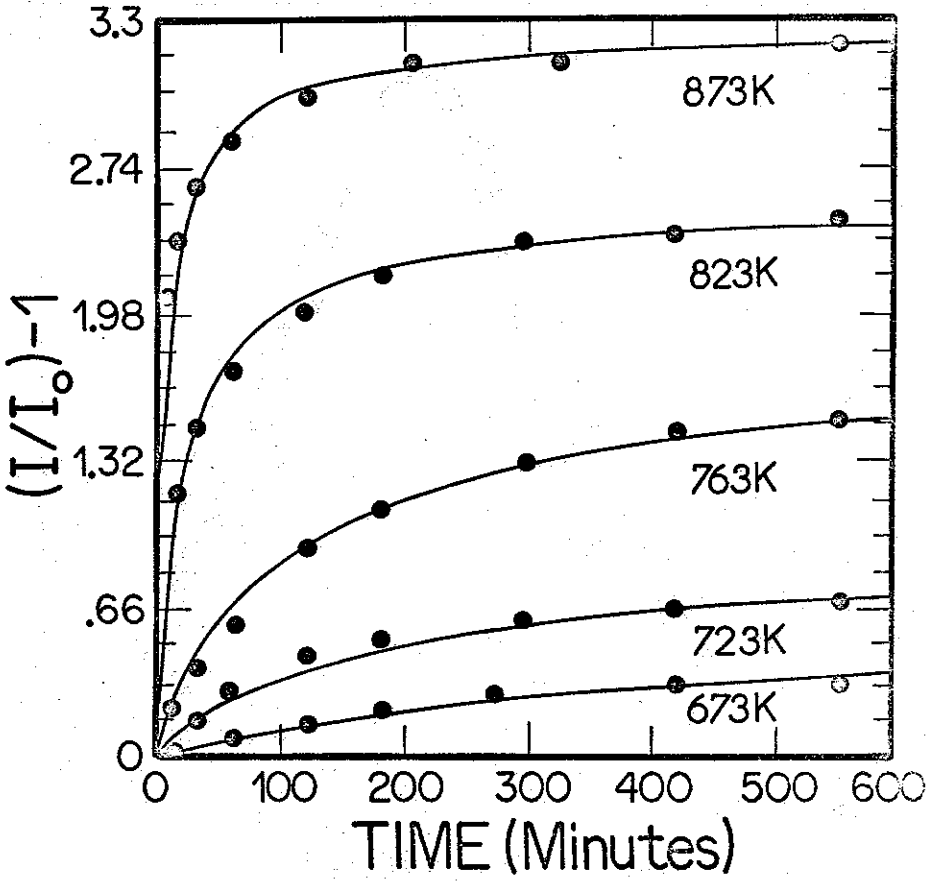

FIGURE 3

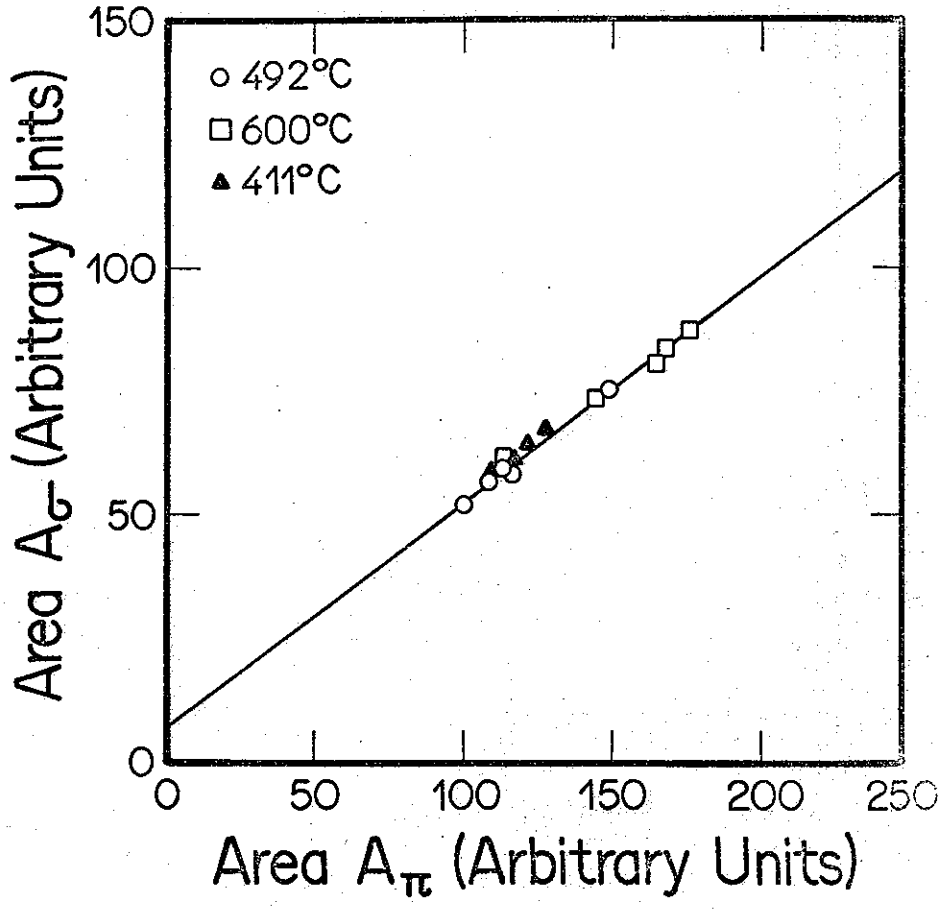

FIGURE 4

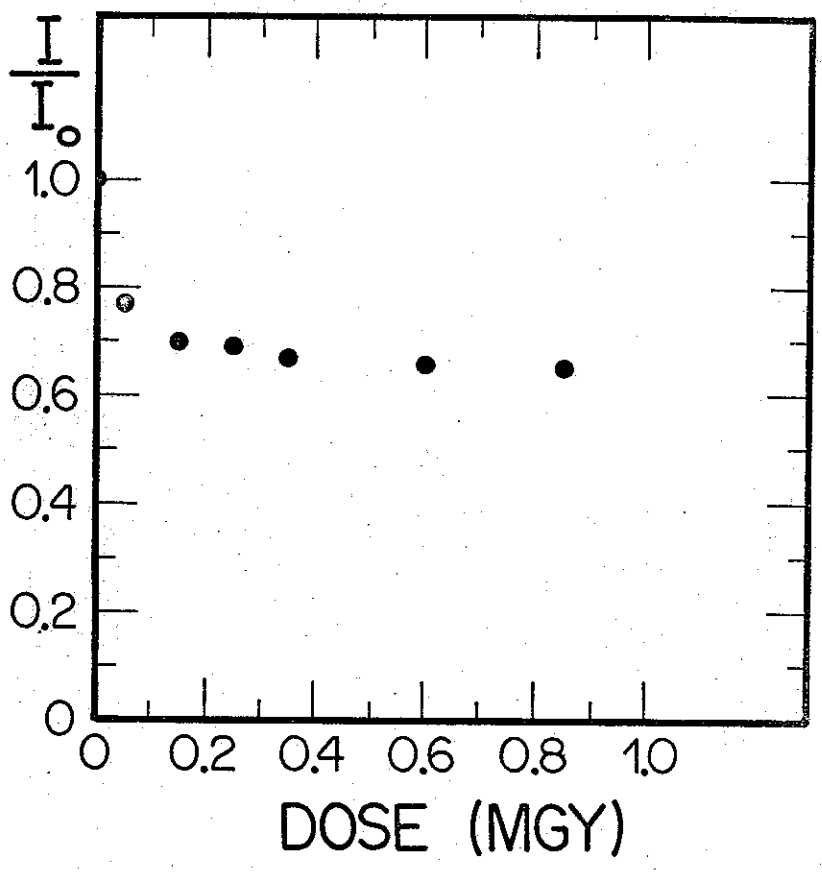

FIGURE 5

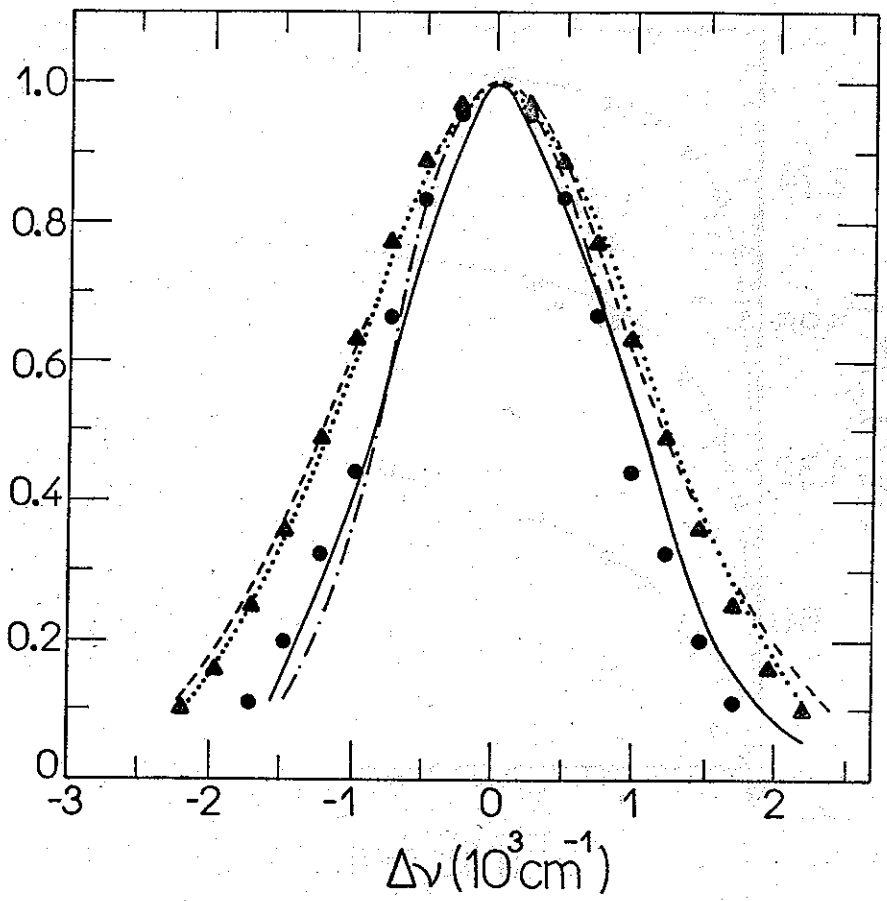

FIGURE 6

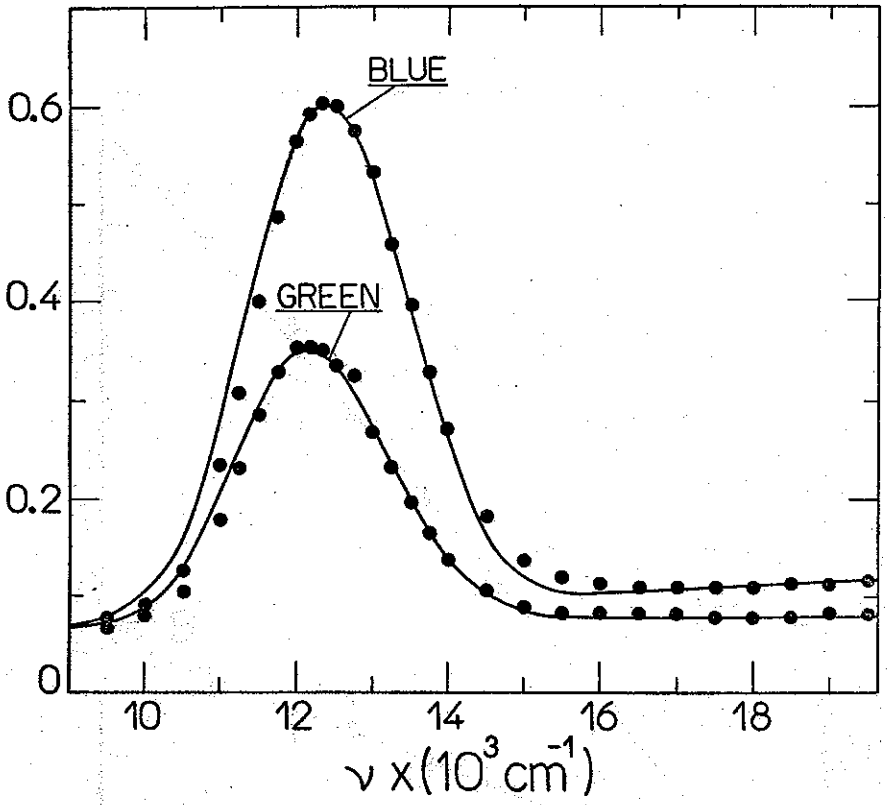

FIGURE 7

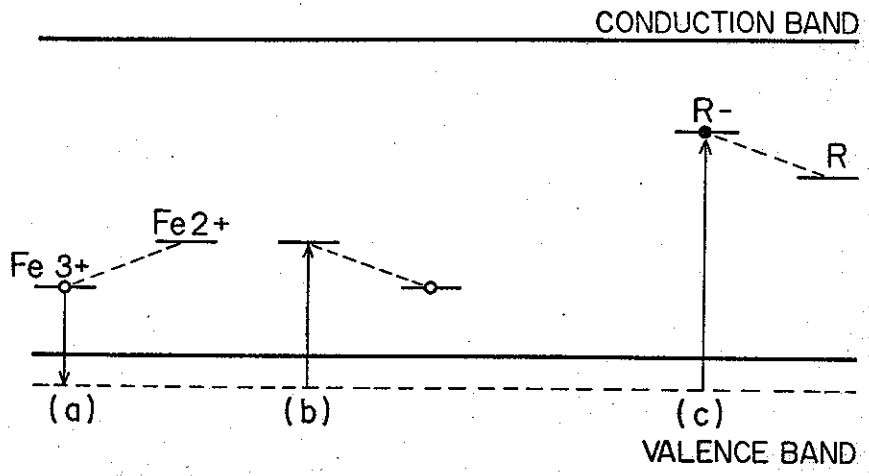

FIGURE 8

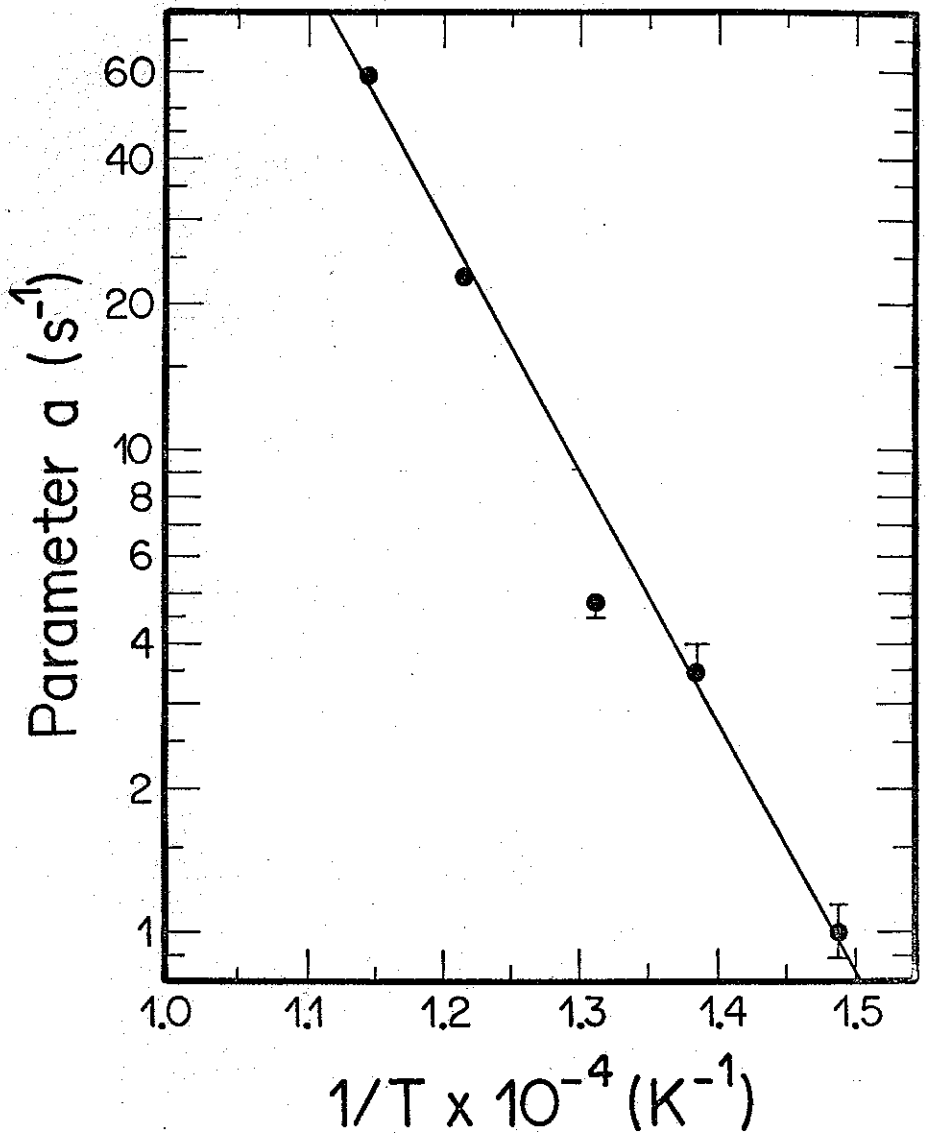

FIGURE 9

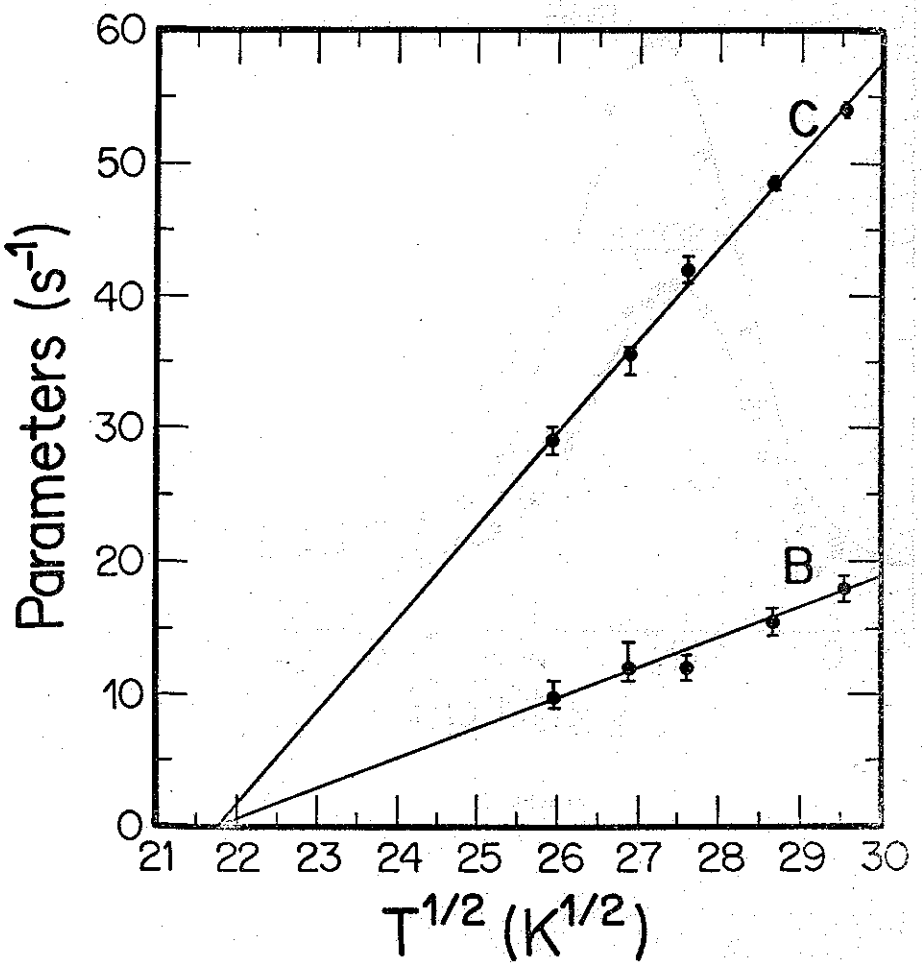

FIGURE 10